Nuclear Instruments and Methods in Physics Research B 267 (2009) 2647–2652

Contents lists available at ScienceDirect

Nuclear Instruments and Methods in Physics Research B

journal homepage: www.elsevier.com/locate/nimb

Calculated depth-dose distributions for H^+ and He^+ beams in liquid water

Rafael Garcia-Molina [a,*], Isabel Abril [b], Cristian D. Denton [b], Santiago Heredia-Avalos [c], Ioanna Kyriakou [d], Dimitris Emfietzoglou [d]

[a] Departamento de Física – CIOyN, Universidad de Murcia, Apartado 4021, E-30080 Murcia, Spain
[b] Departament de Física Aplicada, Universitat d'Alacant, Apartat 99, E-03080 Alacant, Spain
[c] Departament de Física, Enginyeria de Sistemes i Teoria del Senyal, Universitat d'Alacant, Apartat 99, E-03080 Alacant, Spain
[d] Medical Physics Laboratory, University of Ioannina Medical School, Ioannina 451 10, Greece

ARTICLE INFO

Article history:
Available online 27 May 2009

PACS:
34.50.Bw
77.22.−d
87.55.Gh
87.55.K−
87.53.−j

Keywords:
Bragg peak
Liquid water
Depth-dose distributions
Energy loss function
Stopping power
Dielectric formalism
Mean excitation energy

ABSTRACT

We have calculated the dose distribution delivered by proton and helium beams in liquid water as a function of the target-depth, for incident energies in the range 0.5–10 MeV/u. The motion of the projectiles through the stopping medium is simulated by a code that combines Monte Carlo and a finite differences algorithm to consider the electronic stopping power, evaluated in the dielectric framework, and the multiple nuclear scattering with the target nuclei. Changes in projectile charge-state are taken into account dynamically as it moves through the target. We use the MELF–GOS model to describe the energy loss function of liquid water, obtaining a value of 79.4 eV for its mean excitation energy. Our calculated stopping powers and depth-dose distributions are compared with those obtained using other methods to describe the energy loss function of liquid water, such as the extended Drude and the Penn models, as well as with the prediction of the SRIM code and the tables of ICRU.

1. Introduction

The use of fast proton beams for application in radiotherapy was proposed almost sixty years ago [1]. The reason for this lies in that, compared with conventional X-ray beams used so far in therapy, high-velocity protons suffer little angular deflection and have a well-defined penetration range, with a sharp increase in the energy loss at the end of their trajectories. Most of the proton beam energy is deposited at the end of its path in a narrow region (the Bragg peak), while relatively low energy is transferred at the target entrance (the plateau), and only very little energy is released in the tail region beyond the Bragg peak. These features can be used to control the energy delivered to deep tumours in the body, with minimal damage to healthy tissue surrounding the malignant cells. Therefore, the depth-dose curves from proton (and heavier ion) beams are much more efficient for tumour therapy than those from usual photon or electron beams [2,3]. Nevertheless, protons used in therapy applications are, essentially, of low linear energy transfer (LET) and are clinically considered to be by only 10%, i.e. with a relative biological effectiveness (RBE) between 1.1 and 1.15, more cytotoxic than conventional low-LET beams consisting of photons or high-energy electrons. A low-LET beam translates clinically to an oxygen-dependence efficiency of cell-kill which renders hypoxic and otherwise radiation-resistant tumours unresponsive to irradiation. An improved therapeutic efficacy may thus be achieved by ions heavier than protons which, by virtue of their higher charge, exhibit a higher LET and, generally, a higher RBE as well. The challenge here is to limit the high RBE only over the Bragg peak, while keeping a low-LET component throughout both the plateau region and the tail which normally constitute normal tissue. To that end, light ions from helium to carbon have been found most effective for small tumours, while heavier ions (e.g. oxygen nuclei) may be optimal for larger tumours which require a high-LET component over an extended spatial region [4]. Presently, there are about 25 ion therapy facilities throughout the world, the majority of which use proton beams [5].

Liquid water is a substance present in all living matter (70–80% in soft tissue), hence the need for an accurate knowledge of the energy deposition in liquid water by any radiotherapeutic beam.

* Corresponding author.
E-mail address: rgm@um.es (R. Garcia-Molina).

0168-583X/$ - see front matter © 2009 Elsevier B.V. All rights reserved.
doi:10.1016/j.nimb.2009.05.038

Moreover, such calculation is a prerequisite step for modelling the subsequent chemical stage of radiolysis of water which leads to free-radical production; the latter representing a ubiquitous mechanism of radiation-induced biological damage [6].

In this work, we simulate the depth-dose distributions by proton and helium beams in liquid water, for incident energies in the range 0.5–10 MeV/u. The electronic energy loss of a fast-charged projectile is provided by the dielectric formalism [7], with a detailed description of the target energy loss function (ELF) provided by the MELF–GOS model [8,9]. Our results for the depth-dose distributions of proton and alpha particle beams in liquid water will be compared with those obtained by means of other commonly used ELF models [10,11], as well as with the semi-empirical code SRIM 2008 [12].

2. Method

The dielectric extended-optical-data methodology has proved very useful for modelling various aspects of particle-solid interactions and provides an alternative perspective to other successful theories of ion stopping [13]. To account for the electronic excitation spectrum of the target, the first step is to properly describe the energy loss function (ELF) of liquid water in the whole momentum and energy plane ($\hbar k, \hbar\omega$), i.e. the Bethe surface. The ELF enters as a key magnitude in the projectile electronic energy loss formulas [7], and it is provided by $\mathrm{Im}[-1/\varepsilon(k,\omega)]$, where $\varepsilon(k,\omega)$ is the dielectric function of the material. Relatively recent experimental data for the ELF of liquid water in the optical limit ($\hbar k = 0$) and at momentum transfer $\hbar k$ different from zero have become available by means of inelastic X-ray scattering spectroscopy [14–16]; these data are noticeably different from the old reflectance data [17], which pertain to the optical limit ($\hbar k = 0$). The use of these data on proton stopping power calculations in liquid water has been recently examined [18,19]. It was found that the new set of optical data as well as the observed momentum broadening and dispersion of the Bethe ridge have a sizeable effect on the electronic stopping power of protons in the region of the maximum.

In the present work, we have used the MELF–GOS method [8,9] to model analytically the ELF of liquid water, through a fitting to the more recent experimental data [16] in the optical limit ($\hbar k = 0$). The outer-electron excitations of liquid water are fitted by a sum of three Mermin-type ELFs [20], while the contribution of the oxygen K-inner shell is calculated by the GOS method [21]. In Fig. 1, we show our fitting (solid line) and the experimental values (symbols) of the ELF of liquid water in the optical limit, as a function of the energy transfer $\hbar\omega$.

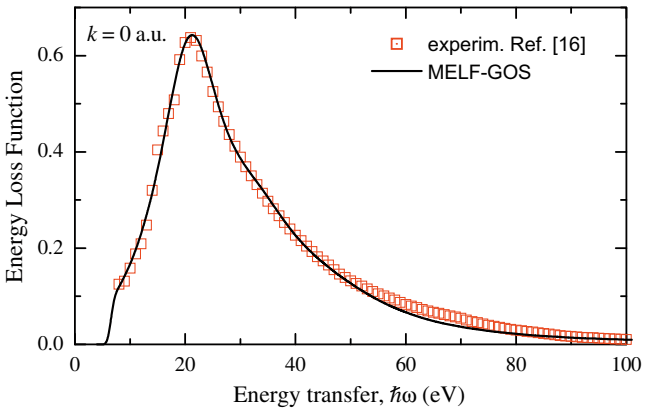

Fig. 1. ELF of liquid water in the optical limit ($\hbar k = 0$) as a function of the transferred energy, $\hbar\omega$. Symbols represent experimental data [16], while the solid curve corresponds to our fitting through the MELF–GOS model. (For interpretation of the references to colour in this figure legend, the reader is referred to the web version of this article.)

Besides appropriately fitting the main characteristics of the experimental ELF at the optical limit, the MELF–GOS method satisfies other physical constrains, such as the f-sum rule (for all values of k) [22]. From the ELF the mean excitation energy I can be calculated [22], for which we obtain 79.4 eV for liquid water. Other values available in the literature are 75 ± 3 eV [23,24], 79.7 ± 2 eV [25,26], 77 eV [27], and 81.8 eV [28], 80.7 eV [29] and 82.4 eV [30] (depending on the database used for oxygen's K-shell optical oscillator strength), 78.4 ± 1 eV [31] and 80.8 ± 2 [32]. As can be seen, a value of ~80 eV for the mean excitation energy of liquid water prevails over the effective value of 67.2 eV used [33] for recent stopping data tables of liquid water [34].

One of the advantages of the MELF–GOS method is that the ELF fitting in the optical limit ($\hbar k = 0$) is analytically and automatically extended to finite momentum transfer ($\hbar k \neq 0$) through the properties of the Mermin dielectric function and the GOS model [35], so an explicit dispersion scheme to incorporate the dependence of the ELF on momentum transfer is not needed. This is particularly important for biomaterials given the almost complete lack of experimental data for $\hbar k > 0$ for this class of materials. In Fig. 2, we compare our ELF of liquid water with experimental results [14] for two different values of the momentum transfer, $\hbar k = 1.18$ a.u. and 3.59 a.u., respectively. Also shown are the results obtained from two extensively used methods to describe the ELF of materials: a sum of Drude-type ELF functions with a quadratic dispersion

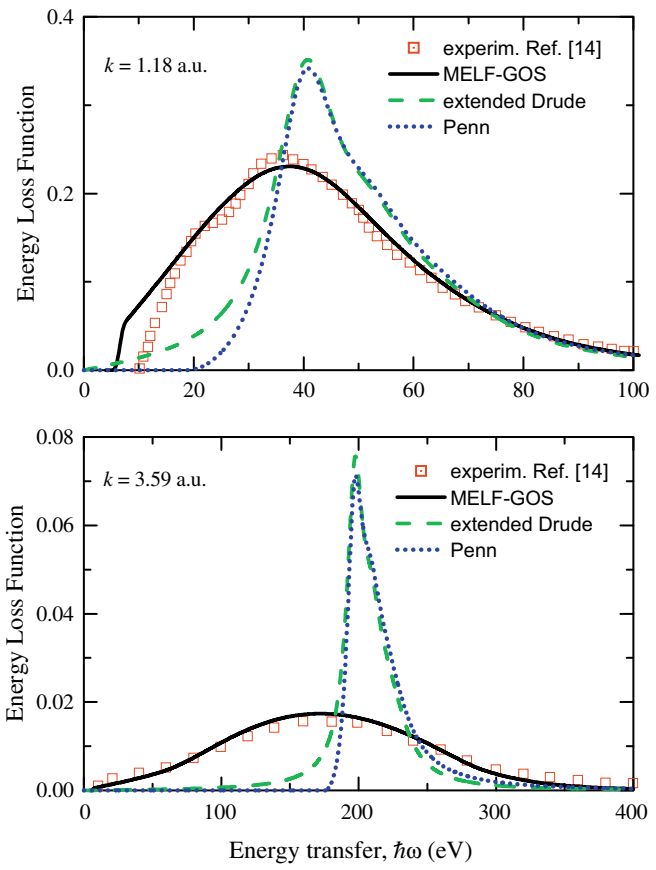

Fig. 2. ELF of liquid water as a function of the energy transfer, $\hbar\omega$, for two values of the wave number: $k = 1.18$ a.u. and 3.59 a.u. Symbols are experimental data [14], and lines represent the results of the different methods used to extend the ELF to finite values of k: MELF–GOS (black solid line), extended Drude (green dashed line) and Penn model (blue dotted line). (For interpretation of the references to colour in this figure legend, the reader is referred to the web version of this article.)

relationship for $\omega(k)$ is assumed in the extended Drude model [10], and a simpler scheme [11] where the sum over a finite number of Drude-type ELFs is replaced by an integration over Lindhard dielectric functions of zero width. It is noteworthy that these three descriptions of the ELF of liquid water are identical in the optical limit, however, the latter two differ appreciably from the former as the momentum transfer increases. It can be observed in Fig. 2 that the MELF–GOS results compare satisfactorily with the experimental data even for $\hbar k$ quite different from zero, whereas the ELF derived from the extended Drude or the Penn models clearly disagree with experiments, as they retain the initial structure of the ELF at $\hbar k = 0$. We have recently presented a comprehensive comparison of the performance of various ELF models for water [36] and have found that the poor performance of most of the available models is to a large extent (but not solely) due to the neglect of the momentum broadening of the ELF, which is here properly accounted for by the Mermin dielectric function [20]. Later on we will see the consequences on the stopping power of the different methods used for ELF extension to finite momentum transfer.

To calculate the energy loss of fast projectiles in liquid water we use the dielectric formalism, which reasonably accounts for the electronic excitations produced in the bombarded materials by the passage of fast particles. At low and intermediate projectile energies it is necessary to consider the processes of electron capture from and loss to the target, which give a continuous charge exchange of the projectile in its path through the solid, accordingly modifying its energy loss. Therefore, for a projectile with atomic number Z_1 and velocity v that bombards a target, the stopping power S_p is obtained mainly as the weighted sum of the partial stopping power, $S_{p,q}$, for each charge q of the projectile [37,38]

$$S_p = \sum_{q=0}^{Z_1} \phi_q S_{p,q}, \tag{1}$$

where ϕ_q is the probability of finding the projectile in a given charge-state q. Since the charge equilibrium is reached in a few femtoseconds after the projectile penetrates into the target, we assume for ϕ_q the charge-state fractions at equilibrium, which depend on the target, the projectile and its velocity. We obtain ϕ_q from the CasP 3.1 code [39]; for compound targets, such as water, this code applies Bragg's rule [40] to their constituents to find the final charge fractions.

The dielectric formalism [7], which is based in the first Born approximation, provides the stopping power of a material, when a projectile with charge-state q and velocity v moves through it, by means of the following integration in the $(\hbar k, \hbar\omega)$ space of target electronic excitations

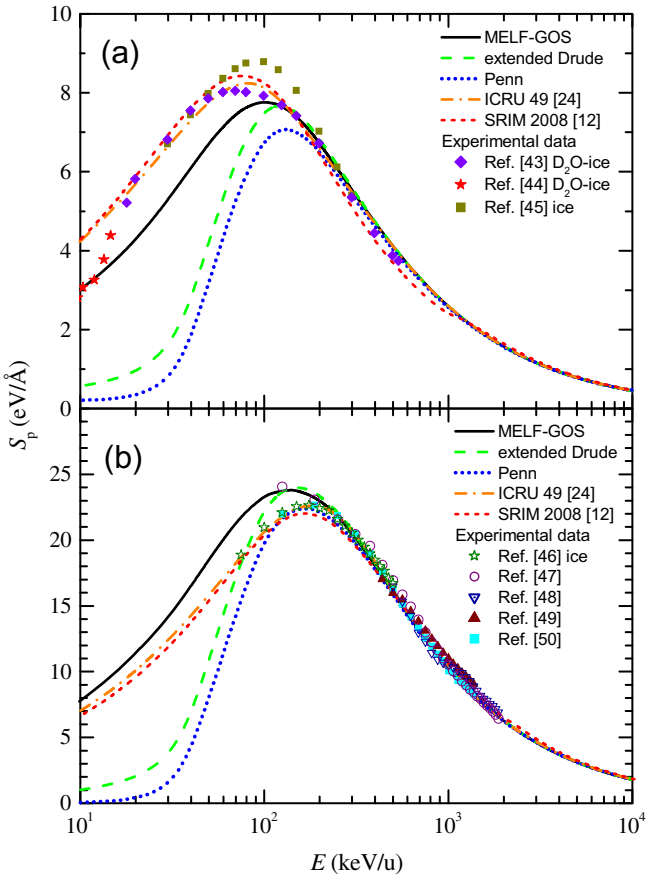

Fig. 3. Stopping power of liquid water for H and He beams, as a function of the incident projectile energy. The curves correspond to present calculations using MELF–GOS model (black solid line), extended Drude model (green dashed line), Penn model (blue dotted line), the results provided by SRIM 2008 (red short dashed line) [12] and the tabulated data of ICRU (orange dash dotted line) [24]. Symbols indicate experimental data, as specified in the inset. Notice that for protons, data are only available for ice, not for liquid water. (For interpretation of the references to colour in this figure legend, the reader is referred to the web version of this article.)

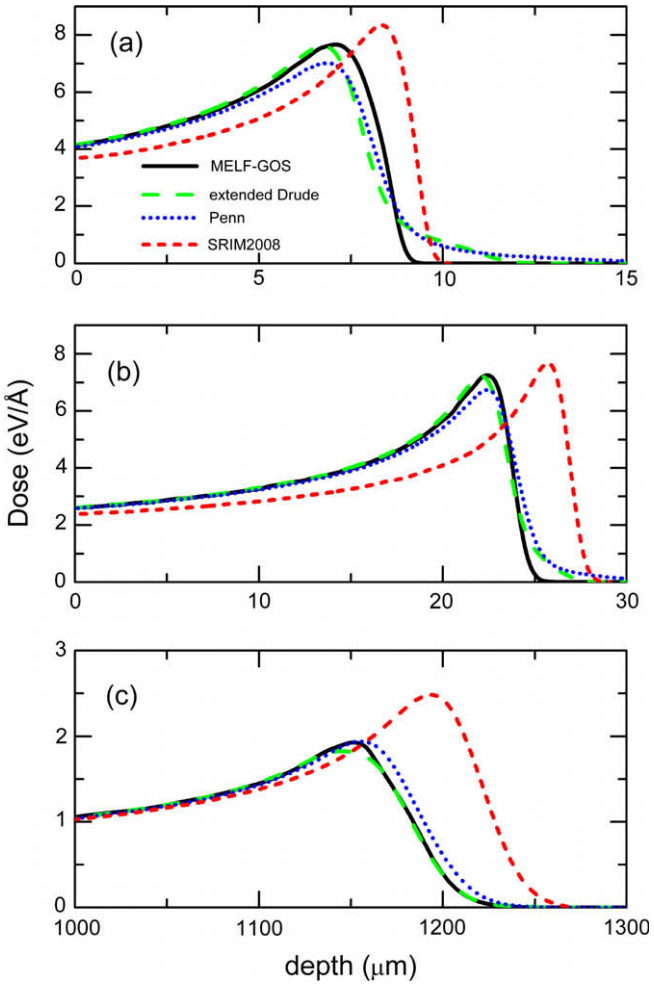

Fig. 4. Depth-dose of proton beams in liquid water as calculated by using the three ELF models: MELF–GOS (black solid line), extended Drude (green dashed line) and Penn (blue dotted line). The SRIM 2008 code [12] is the red short dashed line. Three different projectile energies are considered: (a) 0.5 MeV, (b) 1 MeV and (c) 10 MeV. (For interpretation of the references to colour in this figure legend, the reader is referred to the web version of this article.)

$$S_{p,q} = \frac{2e^2}{\pi v^2}\int_0^\infty \frac{dk}{k}\,\rho_q^2(k)\int_0^{kv} d\omega\ \omega\,\mathrm{Im}\left[\frac{-1}{\varepsilon(k,\omega)}\right]. \quad (2)$$

In the above expression, e is the absolute value of the electron charge, $\rho_q(k)$ is the Fourier transform of the projectile charge density for the charge-state q, and $\mathrm{Im}[-1/\varepsilon(k,\omega)]$ is the ELF of the target. It should be noted that the above formalism overcomes the well-known limitations of Bethe's formula associated with the need for an independent estimate of the shell-corrections and the I-value [41,42]. Other minor contributions to the stopping power, such as electron capture and loss as well as polarization of the projectile cloud are also included, as described in [38].

3. Results and discussion

The calculated stopping powers of liquid water for protons and alpha particles are depicted in Fig. 3, for the three methods previously presented to extend the ELF to the whole momentum and energy space, namely the MELF–GOS [8,9], the extended Drude model [10], and the Penn model [11]. Also depicted are the predictions of the semi-empirical code SRIM [12] and the tabulated data in ICRU [24]. These curves are compared to experimental data [43–50]; it is worth noting that no experimental data for protons in liquid water are available, so we have plotted the data for ice, which clearly differ from those in the vapour phase [24]. At high-energy ($E > 300$ keV/u) all the curves merge into a single one (except for SRIM results for protons, which show a small discontinuity at $E = 1$ MeV), and agreement with experimental data is good for all the calculations. Discrepancies among the curves gradually appear at lower energies ($E < 300$ keV/u), where the results from the extended Drude and the Penn models fall much faster than the MELF–GOS, the SRIM and the ICRU curves. Since the latter two curves are based on slightly different fittings to existing experimental data they are very similar and good agreement with data appears even for low energy projectiles, where our calculated stopping power is ~1 eV/Å smaller than the previous two, although of the same shape. For protons, however, experimental data pertain to ice and not liquid water. Although our calculations are based on the first Born approximation, the standard high-Z corrections associated with the Barkas effect and the Bloch term are negligibly small down to ~100 keV/u [18,19].

The anomalous behaviour at low energies of the stopping power calculated from the extended Drude and the Penn models could be clearly assigned to the poor agreement with experimental data of the corresponding ELF for non-zero momentum transfer, due to the incorrect description of the single-electron excitations at small k, since when the projectile velocity is small it does not produce electronic excitations in the extended Drude or Penn models, in contrast with the MELF–GOS model.

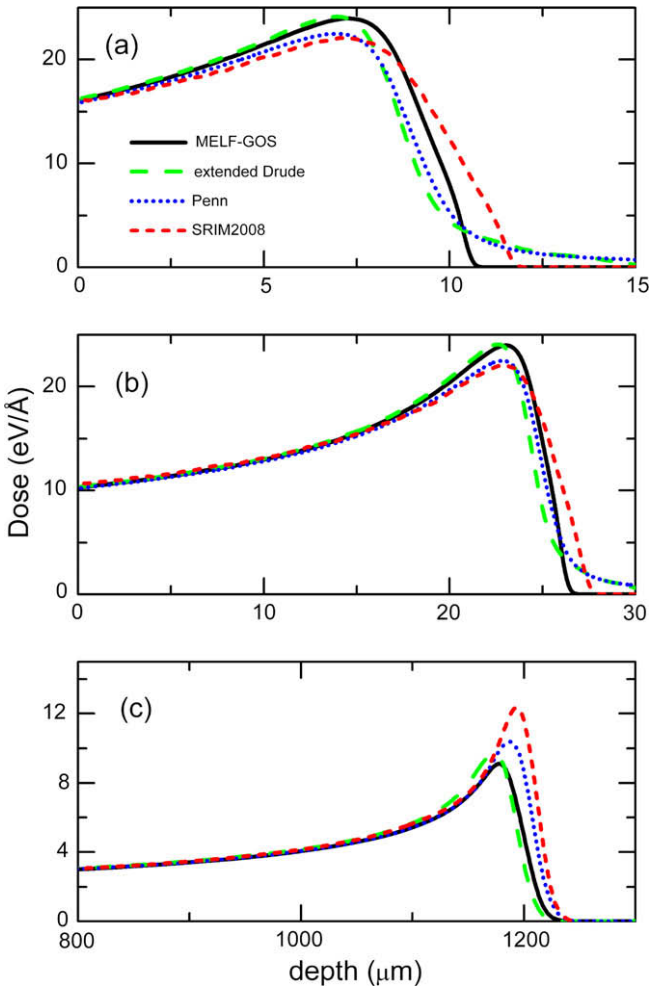

Fig. 5. Depth-dose of helium beams in liquid water as calculated by using the three ELF models: MELF–GOS (black solid line), extended Drude (green dashed line) and Penn (blue dotted line). The SRIM 2008 [12] code is the red short dashed line. Three different projectile energies are considered: (a) 0.5 MeV/u, (b) 1 MeV/u and (c) 10 MeV/u. (For interpretation of the references to colour in this figure legend, the reader is referred to the web version of this article.)

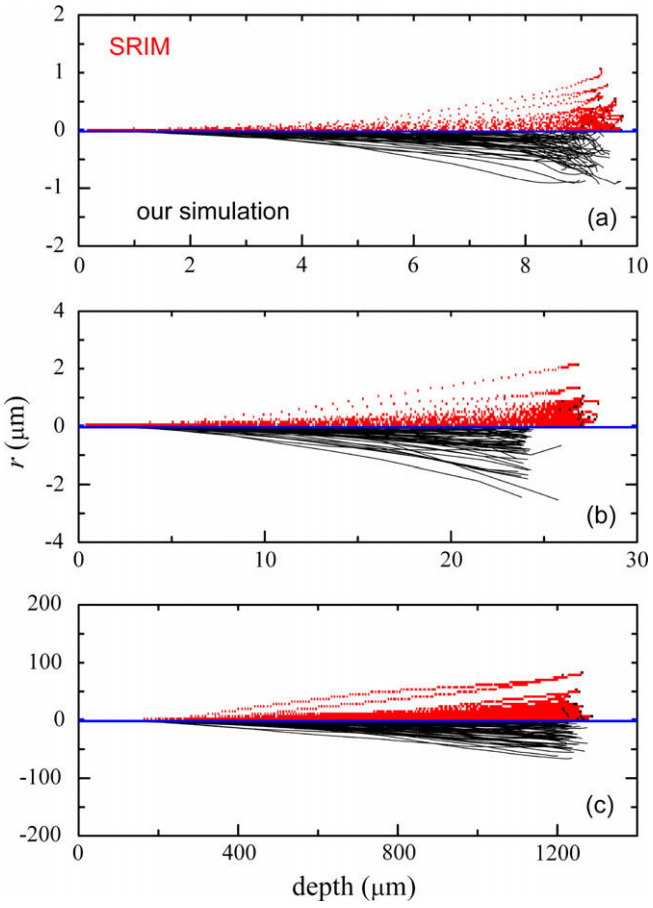

Fig. 6. Simulation of ~100 proton trajectories in liquid water, obtained with the SRIM 2008 code (upper half panels, red lines) and with our simulation code (lower half panels, black lines). Three projectile energies are considered: (a) 0.5 MeV, (b) 1 MeV and (c) 10 MeV. (For interpretation of the references to colour in this figure legend, the reader is referred to the web version of this article.)

Similar comments apply for the stopping power of helium beams in liquid water. Again, all the calculations merge at high energies showing good agreement with experimental data. But now our calculated stopping power from the MELF–GOS model at low energy is ~2 eV/Å higher than ICRU and SRIM 2008 semi-empirical curves, which are fitted to data for ice at the lower energy (~100 keV/u) [46]. It is worth noting the better agreement with liquid water experimental data at ~100 keV/u [47] for the stopping power calculated using the MELF–GOS method.

To calculate the depth-dose distributions for H and He beams in liquid water we use a code [51] that simulates the motion of each projectile through the target. The trajectories of the incident particles are calculated numerically using a finite differences algorithm up to their stop in the target; as the coordinates and velocities of each projectile at each time step are tracked down, the deposited energy of each projectile as a function of the depth can be obtained.

The interaction of the projectile with the target electrons is the main cause of its energy loss at high and intermediate energies. We take into account the electronic energy loss of the projectile through the stopping power, with statistical fluctuations around the mean energy loss due to the energy loss straggling. The electronic energy loss of the projectile depends on its charge-state, velocity and the response of the target. The interactions of the projectile with the target nuclei contribute basically to their angular spread, and at very low energies, when the projectile is close to stopping into the target, to the energy loss. The multiple nuclear scattering is incorporated in the simulation via a Monte Carlo code, where we have used the universal ZBL potential [52] to describe the interaction between the projectile and the atoms that make up the liquid water target. In our simulation, we also consider changes in the projectile charge-state as it moves through the target. The distances between electron capture or loss events as well as their probability are taken from the capture and loss cross-sections according to the mean equilibrium charge-state.

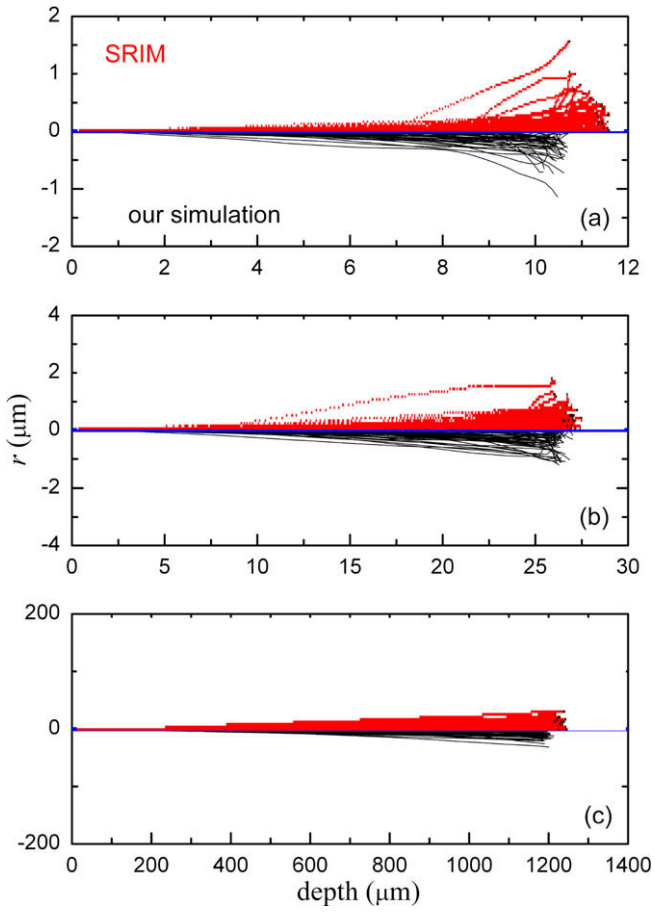

Fig. 7. Simulation of ~100 alpha particle trajectories in liquid water, obtained with the SRIM 2008 code (upper half panels, red lines) and with our simulation code (lower half panels, black lines). Three projectile energies are considered: (a) 0.5 MeV/u, (b) 1 MeV/u and (c) 10 MeV/u. (For interpretation of the references to colour in this figure legend, the reader is referred to the web version of this article.)

The calculated depth-dose distributions in liquid water are depicted in Fig. 4 for H^+ beams and in Fig. 5 for He^+ beams. We can see that the plateau in the dose *vs.* target-depth curve reflects the differences in the stopping powers used in each case (i.e. lower doses are associated to smaller S_p). For the lower energies (0.5 and 1 MeV/u), the intensity of the Bragg peak is comparable for all the calculations, but at the higher energy (10 MeV/u) SRIM results are clearly larger. The simulations obtained with the extended Drude as well as with the Penn models show a tail after the Bragg peak that does not appear in the other calculations. This is due to the rapid fall-off of the stopping power curves at low projectile energies leading to an unphysical extension of the penetration depth. This is a general characteristic applying to all ELF models that predict a sharp Bethe ridge.

Figs. 6 and 7 depict the simulated trajectories of proton and alpha beams, respectively, inside the liquid water target, obtained from the SRIM and the MELF–GOS calculations, respectively; we have restricted simulations to ~100 incident particles for clarity in visualization. The lateral dispersion, *r*, is comparable in both cases, whereas the projected ranges show differences that correlate with the position of the Bragg peak, as a consequence of the different stopping powers used in each calculation.

4. Conclusions

Accurate determination of depth-dose distributions by ion beams is an essential first step to treatment planning considerations. In clinical settings, such information along with the LET distribution over the irradiated tissue is often translated to biological response under some crude assumptions on the LET-dependence of the biological effectiveness. It is generally accepted that to improve the predictive power of present biophysical models of radiation action one needs to accurately quantify the stochastic variation of the actual energy deposition (and not the LET) in the important subcellular target volumes as well as the biological response with respect to these magnitudes. Such efforts would require a full Monte Carlo simulation of the interaction of both the primary ions and all their secondaries (i.e. electrons and nuclear fragments). Efforts along this research are currently underway by many groups [53–56].

In this work, we have used the MELF–GOS model [8,9] to evaluate the stopping power of liquid water for both proton and helium beams. Our calculations compare fairly well with available experimental data and with other commonly used results [12,24]. The value we have obtained for the mean excitation energy, $I = 79.4$ eV, is in better agreement with the trends [32,33] toward a larger value of I than the one presented in the 1993 ICRU Report [24], contrarily to the much lower value of I used in the 2005 ICRU Report [34].

By using a well-established procedure [51], the trajectories of proton and alpha particle beams have been simulated in liquid water, accounting for the different interactions they suffer during their motion inside the target. In this manner, the deposited energy of H and He beams in liquid water as a function of the depth has been calculated, showing the importance of a proper description of the target ELF.

Acknowledgments

This work has been financially supported by the Spanish Ministerio de Educación y Ciencia (Projects Nos. FIS2006-13309-C02-01 and FIS2006-13309-C02-02) and the European Union FP7 ANTICARB (HEALTH-F2-2008-201587). C.D.D. thanks the Spanish Ministerio de Educación y Ciencia for support under the Ramón y Cajal Program.

References

[1] R.R. Wilson, Radiology 47 (1946) 487.
[2] G. Kraft, Prog. Part. Nucl. Phys. 45 (2000) S473.
[3] A.R. Smith, Phys. Med. Biol. 51 (2006) R491.
[4] H. Nikjoo, S. Uehara, D. Emfietzoglou, A. Brahme, New J. Phys. 10 (2008) 075006.
[5] J. Sisterson, Nucl. Instr. and Meth. B 241 (2005) 713.
[6] H. Nikjoo, P. O'Neill, W.E. Wilson, D.T. Goodhead, Radiat. Res. 156 (2001) 577.
[7] J. Lindhard, K. Dan. Vidensk. Selsk. Mat.–Fys. Medd. 28 (8) (1954).
[8] I. Abril, R. Garcia-Molina, C.D. Denton, F.J. Pérez-Pérez, N.R. Arista, Phys. Rev. A 58 (1998) 357.
[9] S. Heredia-Avalos, R. Garcia-Molina, J.M. Fernández-Varea, I. Abril, Phys. Rev. A 72 (2005) 052902.
[10] R.H. Ritchie, A. Howie, Philos. Mag. 36 (1977) 463.
[11] D.R. Penn, Phys. Rev. B 35 (1987) 482.
[12] J.F. Ziegler, J.P. Biersak, SRIM2008, 2008. Available from: <www.srim.org>.
[13] P. Sigmund, Particle Penetration and Radiation Effects. General Aspects and Stopping of Swift Point Charges, Springer-Verlag, Berlin, 2006.
[14] N. Watanabe, H. Hayashi, Y. Udagawa, Bull. Chem. Soc. Jpn. 70 (1997) 719.
[15] H. Hayashi, N. Watanabe, Y. Udagawa, C.-C. Kao, J. Chem. Phys. 108 (1998) 823.
[16] H. Hayashi, N. Watanabe, Y. Udagawa, C.-C. Kao, Proc. Natl. Acad. Sci. USA 97 (2000) 6264.
[17] J.M. Heller, R.N. Hamm Jr., R.D. Birkhoff, L.R. Painter, J. Chem. Phys. 60 (1974) 3483.
[18] D. Emfietzoglou, A. Pathak, G. Papamichael, K. Kostarelos, S. Dhamodaran, N. Sathish, M. Moscovitch, Nucl. Instr. and Meth. B 242 (2006) 55.
[19] D. Emfietzoglou, A. Pathak, H. Nikjoo, Radiat. Prot. Dosim. 126 (2007) 97.
[20] N.D. Mermin, Phys. Rev. B 1 (1970) 2362.
[21] R.F. Egerton, Electron Energy-Loss Spectroscopy in the Electron Microscope, Plenum Press, New York, 1989.
[22] E. Shiles, T. Sasaki, M. Inokuti, D.Y. Smith, Phys. Rev. B 22 (1980) 1612.
[23] ICRU Report 37, Stopping Powers for Electrons and Positrons, International Commission on Radiation Units and Measurements, Bethesda, MD, 1984.
[24] ICRU Report 49, Stopping Powers and Ranges for Protons and Alpha Particles, International Commission on Radiation Units and Measurements, Bethesda, MD, 1993.
[25] H. Bichsel, T. Hiraoka, Nucl. Instr. and Meth. B 66 (1992) 345.
[26] H. Bichsel, T. Hiraoka, K. Omata, Rad. Res. 153 (2000) 208.
[27] M. Krämer, O. Jäkel, T. Haberer, G. Kraft, D. Schardt, U. Weber, Phys. Med. Biol. 45 (2000) 3299.
[28] M. Dingfelder, M. Inokuti, H.G. Paretzke, Rad. Phys. Chem. 59 (2000) 255.
[29] D. Emfietzoglou, H. Nikjoo, Radiat. Res. 163 (2005) 98.
[30] D. Emfietzoglou, F.A. Cucinotta, H. Nikjoo, Radiat. Res. 164 (2005) 202.
[31] Y. Kumazaki, T. Akagi, T. Yanou, D. Suga, Y. Hishikawa, T. Teshima, Rad. Measur. 42 (2007) 1683.
[32] H. Paul, O. Geithner, O. Jäkel, Adv. Quant. Chem. 52 (2007) 289.
[33] H. Paul, ICRU News, 2007 (Letter to the Editor).
[34] ICRU Report 73, Stopping of Ions Heavier than Helium, International Commission on Radiation Units and Measurements, J. ICRU 5 (1) (2005).
[35] D.J. Planes, R. Garcia-Molina, I. Abril, N.R. Arista, J. Electron Spectrosc. Relat. Phenom. 82 (1996) 23.
[36] D. Emfietzoglou, I. Abril, R. Garcia-Molina, I.D. Petsalakis, H. Nikjoo, I. Kyriakou, A. Pathak, Nucl. Instr. and Meth. B 266 (2008) 1154.
[37] S. Heredia-Avalos, R. Garcia-Molina, Nucl. Instr. and Meth. B 193 (2002) 15.
[38] R. Garcia-Molina, I. Abril, C.D. Denton, S. Heredia-Avalos, Nucl. Instr. and Meth. B 249 (2006) 6.
[39] P.L. Grande, G. Schiwietz, CasP. Convolution approximation for swift Particles, version 3.1, 2005. Available from: <http://www.hmi.de/people/schiwietz/casp.html>.
[40] W.H. Bragg, R. Kleeman, Philos. Mag. 10 (1905) 318.
[41] P. Sigmund, Nucl. Instr. and Meth. B 85 (1994) 541.
[42] P. Sigmund, Nucl. Instr. and Meth. B 135 (1998) 1.
[43] W.A. Wenzel, W. Whaling, Phys. Rev. 87 (1952) 499.
[44] D.A. Andrews, G. Newton, J. Phys. D 10 (1977) 845.
[45] P. Bauer, W. Kaferbock, V. Necas, Nucl. Instr. and Meth. B 93 (1994) 132.
[46] S. Matteson, D. Powers, E.K.L. Chau, Phys. Rev. A 15 (1977) 856.
[47] R.B.J. Palmer, A. Akhavan-Rezayat, J. Phys. D 11 (1978) 605.
[48] A. Akhavan-Rezayat, R.B.J. Palmer, J. Phys. E 13 (1980) 877.
[49] D.I. Thwaites, Phys. Med. Biol. 26 (1981) 71.
[50] A.K.M.M. Haque, A. Mohammadi, H. Nikjou, Rad. Prot. Dos. 13 (1985) 71.
[51] S. Heredia-Avalos, R. Garcia-Molina, I. Abril, Phys. Rev. A 76 (2007) 012901.
[52] J.F. Ziegler, J.P. Biersack, U. Littmark, in: J.F. Ziegler (Ed.), The Stopping and Ranges of Ions in Matter, vol. 1, Pergamon, New York, 1985, pp. 1–319.
[53] W. Friedland, P. Jacob, P. Bernhardt, H.G. Paretzke, M. Dingfelder, Radiat. Res. 159 (2003) 101.
[54] H. Nikjoo, S. Uehara, D. Emfietzoglou, F.A. Cucinotta, Radiat. Measur. 41 (2006) 1052.
[55] D. Emfietzoglou, H. Paganetti, G. Papamichael, A. Pathak, Nucl. Instr. and Meth. B 245 (2006) 80.
[56] T. Elsasser, R. Cunrath, M. Kramer, M. Scholz, New J. Phys. 10 (2008) 075005.